Journal of
Materials Chemistry A

Accepted Manuscript

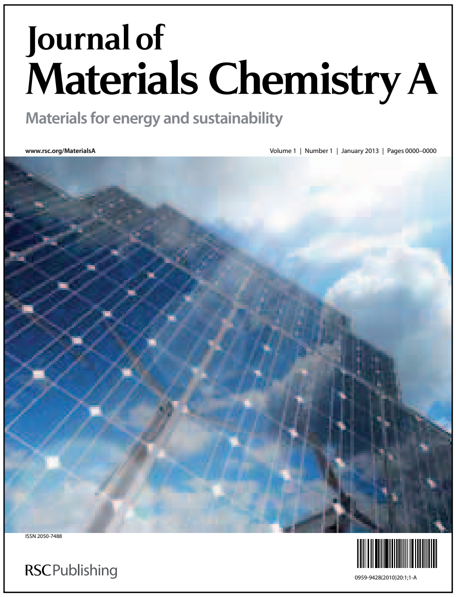

This is an *Accepted Manuscript*, which has been through the RSC Publishing peer review process and has been accepted for publication.

Accepted Manuscripts are published online shortly after acceptance, which is prior to technical editing, formatting and proof reading. This free service from RSC Publishing allows authors to make their results available to the community, in citable form, before publication of the edited article. This *Accepted Manuscript* will be replaced by the edited and formatted *Advance Article* as soon as this is available.

To cite this manuscript please use its permanent Digital Object Identifier (DOI®), which is identical for all formats of publication.

More information about *Accepted Manuscripts* can be found in the **Information for Authors**.

Please note that technical editing may introduce minor changes to the text and/or graphics contained in the manuscript submitted by the author(s) which may alter content, and that the standard **Terms & Conditions** and the **ethical guidelines** that apply to the journal are still applicable. In no event shall the RSC be held responsible for any errors or omissions in these *Accepted Manuscript* manuscripts or any consequences arising from the use of any information contained in them.

RSC Publishing

www.rsc.org/materialsA
Registered Charity Number 207890

Cite this: DOI: 10.1039/c0xx00000x

www.rsc.org/xxxxxx

ARTICLE TYPE

Efficient charge separation and photooxidation on cobalt phosphate-loaded TiO_2 mesocrystal superstructures†

Takashi Tachikawa,*[a,b] Peng Zhang,[a] Zhenfeng Bian[a] and Tetsuro Majima*[a]

Received (in XXX, XXX) Xth XXXXXXXXX 20XX, Accepted Xth XXXXXXXXX 20XX
DOI: 10.1039/b000000x

Development of efficient photocatalysts based on semiconductor materials for organic synthesis, fuel generation, and environmental purification is a central theme in current research and various industries. In this study, we propose a novel strategy for improving the photooxidation activity of photocatalysts by combining metal oxide superstructures and oxygen/hydrogen–evolving co-catalysts. Cobalt phosphate (CoPi) and Pt nanoparticles were selected as model co-catalysts and photochemically deposited on anatase TiO_2 mesocrystals. The structures and reaction dynamics of the composites were thoroughly studied by ensemble-averaged and single-particle spectro-microscopies. Time-resolved diffuse reflectance and electron spin resonance spectroscopy measurements revealed that photogenerated holes in TiO_2 are transferred to the Co species in CoPi upon UV light irradiation. The photooxidation properties of the composites were tested using fluorescence dye probes. It was found that CoPi-loaded TiO_2 mesocrystals had higher activity than standard TiO_2 photocatalysts, and their activity was further enhanced by introducing Pt nanoparticles on specific surfaces. *In situ* fluorescence imaging on a single crystal provides information on the location of reactive sites and the diffusion of product molecules. Consequently, the site-specific modification of co-catalysts tailored by anisotropic electron flow in the mesocrystal superstructures significantly retarded the charge recombination between the holes and electrons, thereby resulting in enhanced (up to approximately 300 times) photooxidation activity.

Introduction

Metal oxide semiconductors have been studied extensively because of their potential applications in photocatalysis, photovoltaics, batteries, and sensors.[1-6] For instance, photocatalytic water splitting into H_2 and O_2 allows for the storage of solar energy as fuel.[5,6] Rapid and efficient collection of multiple electrons (e^-) and holes (h^+) on the catalytic sites of the semiconductor surface to accompany the redox events and bond formation is of paramount importance in the entire reaction sequence. In this regard, surface modification of semiconductors with co-catalysts such as iridium oxides (IrO_x)[7-9] and cobalt oxides/oxyhydroxides (CoO_x/CoOOH)[10-12] has attracted great interest, since such composites are widely applied as efficient photocatalysts to promote oxidation of water. The photocatalytic properties of such composites are known to be strongly influenced by both the method of preparation and the electronic and morphological structures of the semiconductors and co-catalysts. Therefore, understanding the relationship between the structural characteristics and the interfacial charge transfer dynamics allows for optimization of the composite systems, leading to highly improved catalytic performance.

Titanium dioxide (TiO_2) is one of the most promising semiconductors for heterogeneous photocatalysis owing to its low cost, stability, and nontoxicity.[13-16] In general, traditional metal oxide nanoparticles have some limitations in practical applications as photocatalysts and electrode materials because of the rapid recombination of photogenerated e^- and h^+ both in the bulk and on the surface. To overcome this drawback, metal oxide mesocrystals, which have high surface area and highly ordered superstructures composed of metal oxide nanocrystal building blocks, have recently emerged as a new class of porous semiconductor materials.[17-20] Anatase TiO_2 mesocrystal (MesoTiO_2) superstructures could strongly enhance charge separation upon UV light irradiation, yielding remarkably long-lived charges, and consequently, higher photoconductivities and photocatalytic activities.[19,20] However, to the best of our knowledge, there is no report dealing with the fabrication and characterization of photoactive mesocrystal superstructures with oxygen-evolving co-catalysts.

Journal of Materials Chemistry A Accepted Manuscript

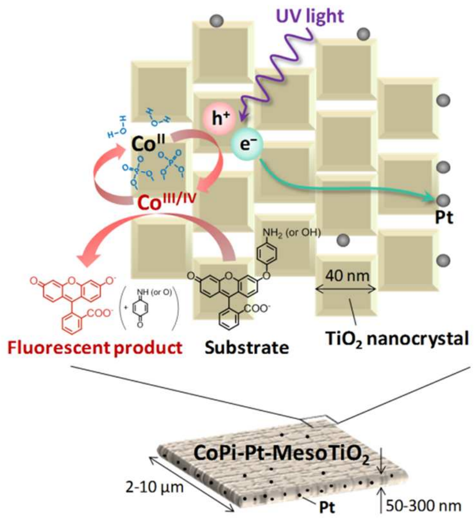

Fig. 1 Schematic illustration of charge transfer on the surface of CoPi-Pt-MesoTiO$_2$. MesoTiO$_2$ is composed of aligned anatase TiO$_2$ nanocrystals. The width and thickness of MesoTiO$_2$ structures are 2–10 μm and 50–300 nm, respectively. Pt nanoparticles are mainly deposited on the lateral surfaces of CoPi-MesoTiO$_2$. Active Co$^{III/IV}$ species in CoPi as well as TiO$_2$ holes (h$^+$) oxidize 3'-*p*-aminophenyl fluorescein (APF) and 3'-*p*-hydroxyphenyl fluorescein (HPF) substrates to generate fluorescein as a fluorescent product and *p*-benzoquinone imine or *p*-benzoquinone as a byproduct, respectively, via *O*-dearylation reaction. TiO$_2$ electrons (e$^-$) migrate to the edges of MesoTiO$_2$ through the TiO$_2$ nanocrystal network, and they are eventually captured by Pt nanoparticles.[20]

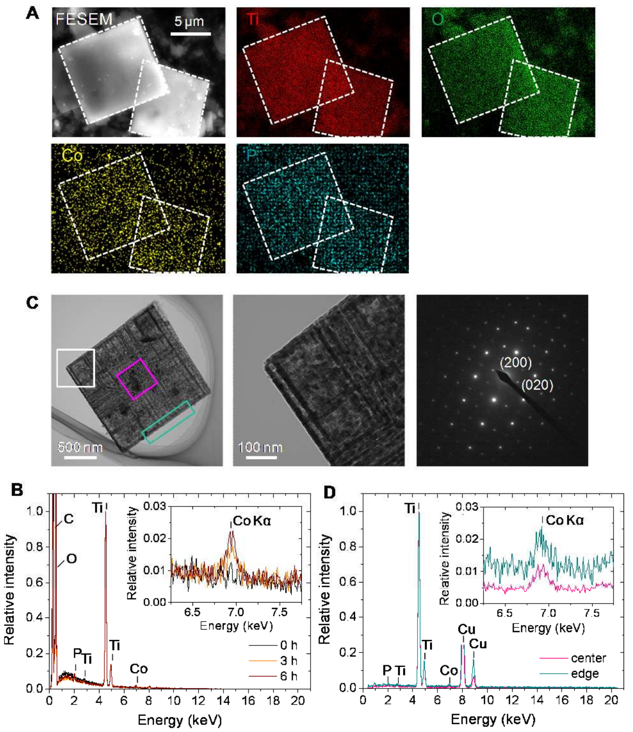

Fig. 2 (A) FESEM and elemental mapping images of CoPi-MesoTiO$_2$. (B) FESEM-EDX spectra of MesoTiO$_2$ after the photodeposition of CoPi for 0, 3, and 6 h. (C) TEM images (left and middle) and diffraction pattern (right) observed for CoPi-MesoTiO$_2$. The middle image represents the enlarged white square in the left image. (D) STEM-EDX spectra measured from the center and edge (which are represented by pink and green squares in TEM image (left), respectively) of CoPi-MesoTiO$_2$ synthesized by photodeposition for 3 h.

As shown in Fig. 1, the plate-like structure of MesoTiO$_2$ is composed of aligned anatase TiO$_2$ nanocrystals with exposed dominant {001} facets. Such a superstructure is beneficial as it allows for the migration of photogenerated e$^-$ between adjacent TiO$_2$ nanocrystals upon UV light irradiation. One possible way to facilitate both charge separation and subsequent water splitting has been the deposition of cobalt phosphate (CoPi),[21,22] known as an efficient oxygen-evolving catalyst, onto semiconductor materials such as ZnO,[11] TiO$_2$,[23,24] Fe$_2$O$_3$,[12,25-28] WO$_3$,[29] and BiVO$_4$.[30,31] It has been considered that the phosphate ions terminate the molecular cobaltate clusters and act as proton acceptor in the oxygen evolution cycle.[24,28] In the present systems, the h$^+$-accepting states of Co species (Co^{II} and Co^{III}) in CoPi are located at energy levels above the valence band (VB) of TiO$_2$. Therefore, upon UV light irradiation, h$^+$ in the TiO$_2$ VB can be transferred to the CoPi catalysts deposited on the surface.[23,24] The e$^-$ in the conduction band (CB) of TiO$_2$ is possibly transferred to the high valence Co ion, eventually inhibiting the oxidation reactions owing to the undesired charge recombination.

Here, we applied a simple photochemical deposition method to modify MesoTiO$_2$ with CoPi and platinum (Pt) nanoparticles, which are commonly used as a co-catalyst for hydrogen evolution, and investigated the reaction dynamics of photogenerated charges in the composite materials by using steady-state and time-resolved spectroscopies. To explore the charge transfer processes in inhomogeneous structures and environments, *in situ* single-particle fluorescence imaging techniques with redox-responsive fluorescence probes were utilized. So far, direct imaging methods based on optical absorption and fluorescence have been applied for screening and optimization of water oxidation catalysts,[32,33] but the present work is the first example of exploring the photooxidation activity of semiconductor-based composites at single-particle or single-aggregate level. It was eventually demonstrated that the photogenerated h$^+$ in MesoTiO$_2$ is effectively trapped by Co species in CoPi, followed by the subsequent oxidation of reaction substrates to fluorescent products. Owing to superior interparticle electron transfer ability, the CoPi and Pt-co-deposited MesoTiO$_2$ composites exhibited up to approximately 300 times higher photoactivity than bare MesoTiO$_2$ and other standard TiO$_2$ photocatalysts.

Results and discussion

Structural characterization

0.1 M phosphate (Pi) buffer suspensions (pH 7.0) containing TiO$_2$ powder and Co^{2+} ions were irradiated by UV light (315–400 nm, 580 mW cm^{-2}) for 3 h to deposit CoPi on the TiO$_2$ surface without any applied bias potential. Fig. 2A shows the field-emission scanning electron microscopy (FESEM) and energy dispersive X-ray (EDX) spectroscopic mapping images of CoPi-

Journal of Materials Chemistry A Accepted Manuscript

This journal is © The Royal Society of Chemistry [year]

Table 1 Structural Characteristics and Photoactivity of CoPi-TiO_2

TiO_2	crystalline phase [a]	particle size (nm) [b]	surface area (m^2 g^{-1}) [b]	deposition time (h)	Co loading (wt%)	relative reaction rate [e]
MesoTiO_2	A	39	63	3	0.69 [c], 0.80 [d]	1.0 (15)
Pt-MesoTiO_2	A	–	–	0.5	1.1 [c], 2.5 [d]	36 (1.6)
P25	A/R	25	55	3	0.42 [c], 0.35 [d]	1.7 (5.1)
ST21	A	20	50	3	0.48 [c], 0.29 [d]	1.6 (5.1)
NanoTiO_2	A	25	41	3	0.49 [c], 0.53 [d]	1.0 (3.5)

[a] A and R mean anatase and rutile, respectively.
[b] Refs. 19 and 20.
[c] Calculated from the absorbance of Co ions in solution.
[d] Obtained from FESEM-EDX analysis.
[e] Calculated from the temporal change of fluorescence intensity for the sample solutions before and after the UV light irradiation. The numbers in parentheses are the enhancements in the reaction rates after the CoPi deposition. See text for details.

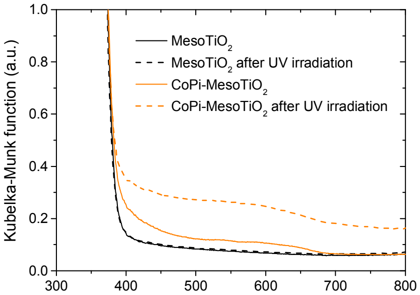

Fig. 3 Steady-state diffuse reflectance spectra of MesoTiO_2 (black) and CoPi-MesoTiO_2 (orange) in phosphate buffer solutions (0.1 M, pH 7.0) before (solid lines) and after (broken lines) 355-nm laser irradiation.

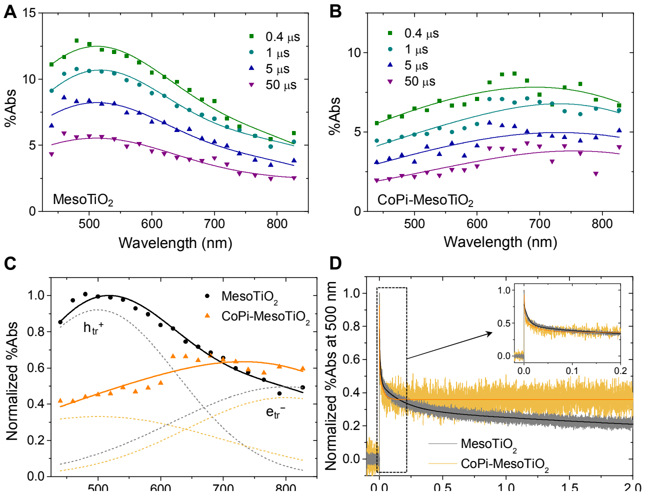

Fig. 4 Time-resolved diffuse reflectance spectra during the 355-nm laser photolysis of MesoTiO_2 (A) and CoPi-MesoTiO_2 (B) in phosphate buffer solutions. Comparisons of transient spectra at 1 μs (C) and time traces at 500 nm (D).

loaded MesoTiO_2 (CoPi-MesoTiO_2). MesoTiO_2 is composed of aligned anatase TiO_2 nanocrystals with an average diameter of around 40 nm, and has a plate-like structure with a width of several micrometers and thickness of around 100 nm. Elemental mapping analysis revealed that Co and P elements are distributed over the surface of MesoTiO_2, and their concentrations are lower than 1 wt%. As shown in Fig. 2B, EDX spectrum obtained from the surface of CoPi-MesoTiO_2 indicates a Co Kα peak, which was not observed for the as-synthesized MesoTiO_2. Transmission electron microscope (TEM) images revealed that CoPi-MesoTiO_2 consists of assembled TiO_2 nanoparticles and that it has many pores on its surface (the left and middle images of Fig. 2C). The electron diffraction pattern of the selected area shows single-crystal diffraction along with the anatase [001] zone axis (the image on the extreme right of Fig. 2C). Scanning TEM (STEM)-EDX spectral measurements were selectively performed for the center and the edge of CoPi-MesoTiO_2, as demonstrated in Fig. 2D, where Ti Kα peaks have been normalized for comparison. Co concentrations are 0.57 ± 0.15 and 0.71 ± 0.35 wt% near the center and the edge of MesoTiO_2, respectively (five different crystals were analyzed).

The concentrations of Co deposited on different TiO_2 samples were further determined by two independent methods as follows: UV-Vis absorption measurements of residual Co^{2+} ions (with a peak at around 520 nm) in solutions after UV light irradiation and FESEM-EDX measurements. The concentrations of deposited Co under the same synthesis conditions are summarized in Table 1 along with the structural characteristics of TiO_2 used in this study. To facilitate the comparison, two TiO_2 samples with the anatase crystal phase were used, commercial TiO_2 (ST21) and synthesized TiO_2 (NanoTiO_2) nanocrystals. NanoTiO_2 has a truncated bipyramidal morphology with dominant {001} facets, analogous to the TiO_2 nanocrystal building blocks of MesoTiO_2.[19] P25 consists of anatase and rutile crystalline phases and is frequently used as a benchmark in photocatalysis.

From Table 1, it is evident that Co species can be deposited more effectively on the surface of MesoTiO_2 than on the surface of other TiO_2 nanocrystals. During photochemical deposition, h^+ in the TiO_2 VB is used to oxidize Co^{2+} ions to deposit Co^{III} species as an oxide or as oxyhydroxides on the TiO_2 surface, while e^- in the TiO_2 CB reduces the Co^{III} species back to the starting Co^{II} material.[23,24] Therefore, the highest deposition ability of MesoTiO_2 is possibly due to the efficient charge separation owing to the ordered structure of TiO_2 nanocrystals. In addition, Pt nanoparticle-loaded MesoTiO_2 (Pt-MesoTiO_2), with Pt nanoparticles of ~3 nm mostly located on the lateral surfaces containing {101} facets of MesoTiO_2,[20] was found to be more efficient for the deposition of Co species on the surface (Fig. S1and S2†). Pt nanoparticles loaded on TiO_2 could collect e^-, and thus greatly improve the oxidation efficiency, enhancing significantly the photochemical deposition of the Co species.

Journal of Materials Chemistry A Accepted Manuscript

Table 2 Decay Time Constants of Transient Absorption at 500 nm

TiO_2	lifetime (ms) [a]
MesoTiO_2	0.009 (39%), 0.18 (22%), 5.7 (39%),
CoPi-MesoTiO_2	0.0015 (54%), 0.026 (16%), >10 (30%)

[a] Determined by the non-linear least squares curve fitting. The numbers in parentheses are relative amplitudes.

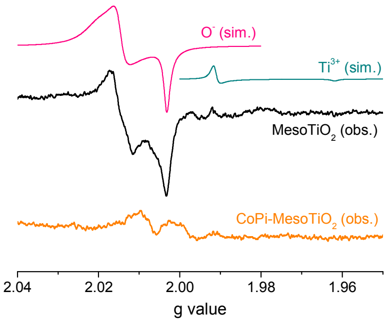

Fig. 5 Differential EPR spectra for MesoTiO_2 (black line) and CoPi-MesoTiO_2 (red line) in frozen buffer solutions, obtained by subtracting the spectra observed before the UV light irradiation from those after the UV light irradiation at 77 K. "Obs." and "sim." are the observed and simulated spectra, respectively. To reproduce the observed spectra, simulations were performed with the following EPR parameters: g_{xx} = 2.0205, g_{yy} = 2.0015, g_{zz} = 2.0035 for O^- and $g_{\parallel}$ = 1.9915, $g_{\perp}$ = 1.9620 for Ti^{3+}.

Time-resolved diffuse reflectance spectroscopy

Fig. 3 shows the steady-state UV-Vis diffuse reflectance spectra of MesoTiO_2 (black solid line) and CoPi-MesoTiO_2 (orange solid line). CoPi-MesoTiO_2 sample displayed broad absorption covering the visible range, in addition to the strong absorption by TiO_2 in the UV region. Co oxides and oxyhydroxides with Co^{II} or Co^{III} states are known to have light-yellow or gray color, respectively,[34] which are in accordance with the observed spectra for CoPi-MesoTiO_2.

Time-resolved diffuse reflectance spectroscopy was employed to explore the reaction dynamics of photogenerated e^- and h^+ in TiO_2. As seen in Fig. 4A, MesoTiO_2 exhibits a broad transient absorption band in the visible to near-infrared range upon 355-nm laser excitation, which represents the overlapping of trapped h^+ (mainly 400–700 nm) and trapped e^- (mainly 500–850 nm).[35,36] Fig. 4C compares the transient absorption spectra observed at 1 µs in the presence and absence of CoPi on MesoTiO_2. From spectral deconvolution into individual components, it was found that the presence of CoPi decreases the absorption intensity of trapped h^+ at around 500 nm (also see Fig. 4B for the spectra at different time regions). These results suggest that photogenerated (free and trapped) h^+ is transferred to the Co^{II} or Co^{III} species on the TiO_2 surface.

Cowan *et al.* observed long-time-scale bleaching at 580 nm for CoPi-Fe_2O_3 nanoparticles by time-resolved diffuse reflectance spectroscopy.[37] They explained this phenomenon in terms of the depletion of photogenerated h^+ in Fe_2O_3 by the transfer to Co, or losing the characteristic optical absorption of Co^{II} or Co^{III} species. The decay profiles at 500 nm were analyzed by multi-exponential curve fitting and the determined lifetimes are summarized in Table 2. By CoPi deposition, the lifetimes of trapped h^+ shortened significantly compared with those in pure MesoTiO_2, and a new long-lived component with lifetime of >10 ms appeared. Furthermore, we noticed that the color of CoPi-MesoTiO_2 suspension changed from pale yellow to dark blue upon the laser irradiation. This color change was significantly suppressed by saturating the suspension with oxygen gas (electron scavenger) before the UV light irradiation. Steady-state diffuse reflectance measurements confirmed that a broad absorption band emerged in the 400–800 nm wavelength region when CoPi-MesoTiO_2 powder in phosphate buffer solution was exposed to 355-nm laser light (Fig. 3). This resembles a well-known feature of e^- accumulated in TiO_2,[38,39] inferring that the observed non-decay component can be ascribed to the prolonged lifetime of trapped e^-.

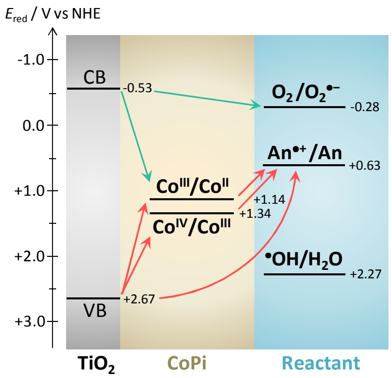

Fig. 6 Energy diagram for the interfacial charge transfer on CoPi-TiO_2.[44] CB and VB are conduction and valence bands of TiO_2, respectively. The band potentials are calculated from $E_{CB} = -0.12 - 0.059 \cdot pH$ and band gap energy of 3.2 eV.[45] "An" is aniline,[46] which is the preferable moiety for the oxidation of APF. The redox potential (E_{red}) of phenol, which is the preferable moiety for the oxidation of HPF, is +0.86 V vs. NHE.[47]

EPR spectroscopy

The photoinduced charge transfer processes in CoPi-MesoTiO_2 were also confirmed by electron paramagnetic resonance (EPR) spectroscopy. EPR spectra of the samples were taken at 77 K before and after the UV light irradiation for 20 min at 77 K, and are given as differential EPR spectra in Fig. 5. The spectrum of MesoTiO_2 exhibits intense resonance peaks at g = 2.017, 2.012, and 2.003. This spectral feature has been assigned to the trapped h^+, *i.e.*, O^- in TiO_2, as reproduced from the reported EPR parameters (pink solid line).[40,41] The very weak resonance signal at g = 1.992 could be attributed to the trapped e^-, *i.e.*, Ti^{3+} in bulk.[42] This Ti^{3+} signal is known to weaken upon annealing at >250 °C in air (MesoTiO_2 used in this study was annealed at 500 °C during the synthesis).[43] On the other hand, the spectrum of CoPi-MesoTiO_2 has no assignable peaks related to the trapped charges in TiO_2. Although the EPR signals of Co species were not observed in the magnetic field range of 80□580 mT,[44] possibly due to their low concentrations, our observation suggests that photogenerated h^+ is scavenged by the CoPi deposited on the TiO_2 surface.

Photooxidation activity

The energy diagram for the charge transfer on CoPi-TiO_2 surface is illustrated in Fig. 6. The hole transfer from excited TiO_2 to

Journal of Materials Chemistry A Accepted Manuscript

This journal is © The Royal Society of Chemistry [year]

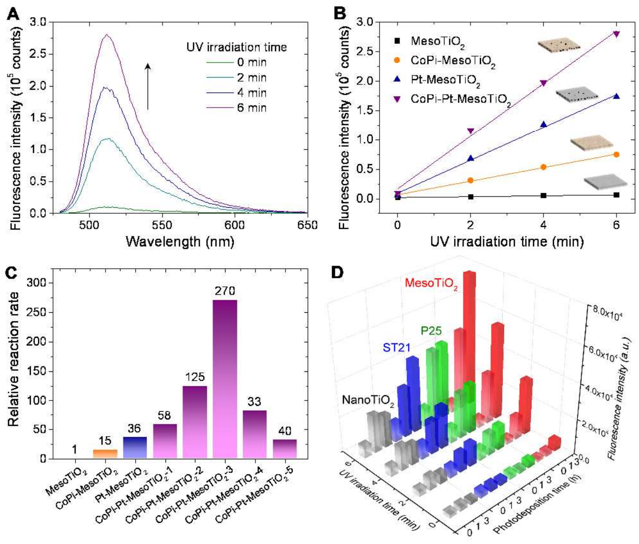

Fig. 7 (A) Fluorescence spectra of phosphate buffer solutions (0.1 M, pH 7.0) before and after the UV light irradiation of sample suspensions containing CoPi-Pt-MesoTiO$_2$ (0.07 g L^{-1}), APF (2 µM), and DMSO (100 mM) as an $^{\bullet}$OH scavenger (excitation at 470 nm). TiO$_2$ powder was removed by centrifugation before the measurements. (B) UV light irradiation time dependence of fluorescence intensities monitored at 512 nm. In the illustrated structures of the samples, MesoTiO$_2$ and CoPi-MesoTiO$_2$ are shown in gray and ivory, respectively. Black dots indicate the Pt nanoparticles deposited on the surface. (C) Relative reaction rates obtained for MesoTiO$_2$-based samples. The reaction rates were determined from the initial slopes of fluorescence intensity changes. The *n* of CoPi-Pt-MesoTiO$_2$-*n* (*n* = 1–5) is the number of repetitions for the CoPi deposition ([MesoTiO$_2$] = 1 g L^{-1}, [Co^{2+}] = 0.5 mM, UV light irradiation time = 30 min). Each procedure can deposit ~1.1 wt% Co (estimated from UV-Vis absorption measurements) on the MesoTiO$_2$ surfaces. (D) Dependence of fluorescence intensity on the UV light irradiation time and photodeposition time for phosphate buffer solutions containing the reaction products.

Co$^{II/III}$ species is thermodynamically possible, and this process enhances the efficiency of photoinduced charge separation, thereby ensuring substantial enhancement in photocatalytic activity for redox reactions. The photooxidation activity of bare TiO$_2$ and CoPi-TiO$_2$ was first evaluated by using ensemble-averaged spectroscopy. We used two fluorescence dye probes, 3'-*p*-aminophenyl fluorescein (APF) and 3'-*p*-hydroxyphenyl fluorescein (HPF), to monitor the oxidation reaction. For instance, upon the oxidation of *p*-aminophenyl group of APF by TiO$_2$ h$^+$ or active Co$^{III/IV}$ species, APF produces fluorescein as a main fluorescent product and *p*-benzoquinone imine as a byproduct (*p*-benzoquinone for HPF) via oxidative *O*-dearylation reactions (Fig. 1 and 6). Based on product analysis, a possible reaction mechanism is proposed in the ESI.

In bulk experiments, TiO$_2$ powder (0.07 g L^{-1}) dispersed in 3 mL of 2 µM APF phosphate buffer solution (pH 7.0) was irradiated in a 1 cm × 1 cm quartz cell by UV lamp (centered at 365 nm, 6 mW cm^{-2}). Dimethyl sulfoxide (DMSO) (100 mM) was added to the sample solution to scavenge $^{\bullet}$OH, which is highly reactive oxygen species generated during the TiO$_2$ photocatalytic reactions.[48] As shown in Fig. 7A, after UV light irradiation of CoPi and Pt nanoparticle-loaded MesoTiO$_2$ (CoPi-Pt-MesoTiO$_2$) sample, the fluorescence intensity of the peak at 512 nm gradually increased, indicating the generation of fluorescein. Fig. 7B shows the time course of the fluorescence intensity for the MesoTiO$_2$-based samples during UV light irradiation. In the absence of TiO$_2$ or UV light, the increase in the fluorescence intensity due to the UV light-induced oxidation or auto-oxidation of APF is almost negligible. The photocatalytic activity of CoPi-Pt-MesoTiO$_2$ remains well after repeated use, ensuring its durability (Fig. S4†). The oxidation reactivity followed the order CoPi-Pt-MesoTiO$_2$ > Pt-MesoTiO$_2$ > CoPi-MesoTiO$_2$ > MesoTiO$_2$. The deposition of Pt nanoparticles greatly enhances the activity, because part of e$^-$ in TiO$_2$ is transferred to Pt before the charge recombination, thus increasing the concentration and lifetime of h$^+$ in TiO$_2$. The repeated deposition of CoPi on Pt-MesoTiO$_2$ enhances the photooxidation by an order of magnitude (Fig. 7C). Excess amount of CoPi caused a decrease in the activity, probably due to the deactivation of Co$^{III/IV}$ species by capturing e$^-$. We also compared the activity of CoPi-MesoTiO$_2$ with those of the TiO$_2$ nanocrystal reference samples. As demonstrated in Fig. 7D, CoPi-loaded MesoTiO$_2$ showed the highest fluorescence intensity and activity enhancement among the tested TiO$_2$ samples, thus highlighting the importance of the ordered structure of MesoTiO$_2$, especially when compared with NanoTiO$_2$ (see also Table 1).

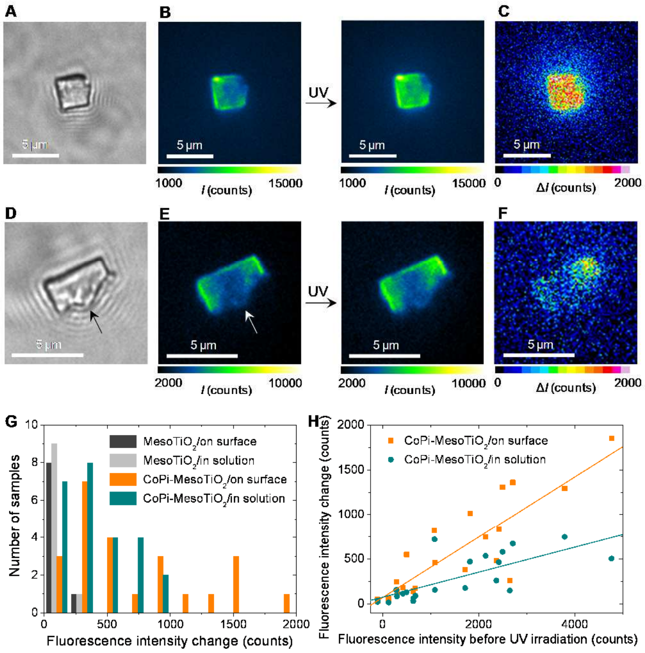

Fig. 8 Optical transmission (A,D) and fluorescence (B,E) images of single CoPi-MesoTiO$_2$ crystals before and after the UV light irradiation. The arrows in the panels D and E indicate the disordered part of the mesocrystal. (C,F) Differential fluorescence images obtained by subtracting the image before the UV light irradiation from the image just after the UV light irradiation. The acquisition time for one frame was 50 ms. (G) Histograms of UV light-induced change in fluorescence intensity measured on the surface of the crystal and in solution at the distance of 1 µm from the edge of the crystal. (H) The relationship between the initial fluorescence intensity and UV light-induced fluorescence intensity change. The background was subtracted from the original data.

Single-particle fluorescence imaging

Based on the results above, we have evaluated the photooxidation activity of individual CoPi-MesoTiO$_2$ crystals by *in situ* fluorescence imaging. Experiments on a single crystal provide

Journal of Materials Chemistry A Accepted Manuscript

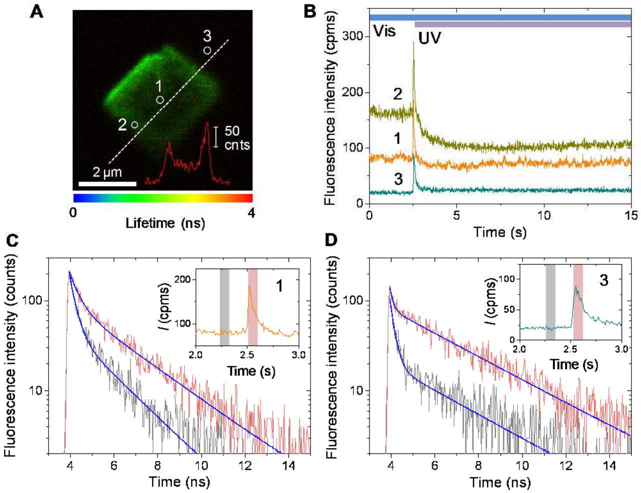

Fig. 9 (A) Fluorescence lifetime image of CoPi-MesoTiO_2 in phosphate buffer solution (0.1 M, pH 7.0) containing HPF (2 μM) and DMSO (100 mM) during 485 nm laser irradiation. The line profile of the fluorescence intensity obtained along the broken line is shown in red. (B) Time traces of fluorescence intensity measured on the center and the edge of the crystal as well as in solution at the distance of 1 μm from the edge of the crystal (see the panel A). Fluorescence decay profiles measured on the center of the crystal (C) and in solution (D) before (gray) and after (red) UV light irradiation. Insets indicate the analyzed time regions in the time traces of fluorescence intensity (see the panel B).

Table 3 Fluorescence Lifetimes of Substrates and Products on CoPi-MesoTiO_2 and Reference Compounds

sample	location	UV light	fluorescence lifetime (ns) [a]
CoPi-MesoTiO_2/HPF	surface	off	0.28 (77%), 1.8 (23%)
		on	0.41 (58%), 2.5 (42%)
	solution	off	0.20 (82%), 3.2 (18%) [b]
		on	0.14 (43%), 3.3 (57%) [b]
		off	0.13 (87%), 3.7 (13%) [c]
		on	0.14 (74%), 3.8 (26%) [c]
HPF	solution	off	0.14 (86%), 4.0 (14%)
		on	0.14 (86%), 4.0 (14%)
Fluorescein	solution	off	4.0 (100%)

[a] The numbers in parentheses are relative amplitudes.
[b] Measured at the 1 μm distance from the edge of the crystal.
[c] Measured at the 10 μm distance from the surface of the crystal.

useful information for elucidating the inherent heterogeneity of the reaction processes on surfaces.[49,50] Fig. 8A and B show typical optical transmission and fluorescence images of a single CoPi-MesoTiO_2 crystal in 2 μM HPF phosphate buffer solution (0.1 M, pH 7.0), respectively. The crystal was illuminated by the evanescent light of 488-nm continuous wave laser (penetration depth is ~200 nm) or 365-nm LED light to excite the fluorescence dye or TiO_2, respectively. The initial fluorescence observed prior to the UV light irradiation is ascribed to the HPF molecules adsorbed on the surface. Under our experimental conditions, the contributions of the scattered light from the crystal and the fluorescence from the photooxidation products directly formed by UV light irradiation are negligible due to the low excitation intensity (~3 W cm^{-2} and ~5 mW cm^{-2} at the cover glass surface for 488 nm and 365 nm light, respectively).[46,48] Interestingly, the area near the edge of the CoPi-MesoTiO_2 crystal showed higher fluorescence intensity than that near the center (Fig. 8B and 9A, respectively). The average intensity ratio of the edge (within 1 μm distance from the lateral faces) and the center is 1.4 ± 0.2, which is greater than that (1.1 ± 0.1) of the bare MesoTiO_2. Previously, it was demonstrated by site-selective deposition of Pt nanoparticles and single-molecule fluorescence imaging of reduction sites with a specific fluorogenic probe that the photogenerated e^- in MesoTiO_2 can reach the lateral surfaces over a micrometer distance through the nanocrystal network.[20] Assuming that fluorescence intensity correlates directly with the number of adsorbed HPF molecules, the observed spatial distribution of fluorescence intensity implies that Co species are readily deposited on the basal surfaces near the edges of MesoTiO_2, and their concentration gradually decreases towards the center. This tendency was also confirmed by the STEM-EDX analysis (Fig. 2D). Moreover, it is obvious from the transmission and fluorescence images (Fig. 8D and E) that the well-structured parts of MesoTiO_2 exhibit higher fluorescence intensity, *i.e.*, higher concentration of Co species, than the disordered parts of MesoTiO_2. From the TEM analysis, it was also found that Pt nanoparticles are deposited more effectively on the edge of the well-ordered parts of MesoTiO_2 than on the edge of the disordered parts of MesoTiO_2 (Fig. S1†). Although it is difficult to observe selectively the reaction processes on the basal and lateral surfaces of CoPi-MesoTiO_2 because of the limited spatial resolution (~250 nm), our findings support the hypothesis that well-ordered structures of MesoTiO_2 can effectively deliver e^- to the lateral surfaces, thereby increasing the oxidation reaction efficiency.

As predicted by the ensemble experiments, the fluorescence intensity on the crystal underwent a substantial increase immediately after the UV light irradiation (Fig. 8C and F). Moreover, the UV light-induced increase in fluorescence intensity around the perimeter of the crystal indicates that the fluorescent products diffused from the crystal surface into the bulk solution. This result supports the proposed mechanism for the oxidation of the probes (Fig. 1 and S3†), and it is well consistent with the fact that more than 90% of fluorescent products are separated from the sample suspensions by centrifugation or filtration, possibly owing to the electrostatic repulsion between negatively charged TiO_2 surface (isoelectric point ≈ 5.5) and fluorescein dianion (pKa 6.4) in water at pH 7.0.[51] Considering the pore size distribution of MesoTiO_2 (5.1 ± 2.5 nm)[19] and the hydrodynamic radius of fluorescein (0.8 nm),[52] the escape of the product fluorescein molecules into the bulk solution should however be partially restricted, allowing us to observe the change in fluorescence intensity over the crystal. The change in the fluorescence intensity varies strongly from crystal to crystal, as shown in Fig. 8G. Meaningful positive correlation was observed for the initial fluorescence intensity with UV light-induced fluorescence intensity changes on the surface (corrected $R^2 = 0.72$) and in solution near the crystal (corrected $R^2 = 0.51$) (Fig. 8H), again indicating the photooxidation of preadsorbed HPF molecules.

Space- and time-resolved confocal fluorescence measurements for individual crystals provided further insight into the mechanism of photooxidation reactions. As demonstrated in Fig. 9A, the fluorescence lifetime measured for CoPi-MesoTiO_2 in 2 μM HPF buffer solution was approximately 1.5 ns, and it was nearly homogeneous over the entire crystal. Similar tendency was observed for more than four individual crystals. This result infers that the spatial distribution of fluorescence intensity is likely due

Journal of Materials Chemistry A Accepted Manuscript

to the differences in the local concentrations of HPF molecules on the surface, not due to the differences in fluorescence lifetimes. We analyzed the temporal changes of the fluorescence intensity and lifetime at different locations on the crystal upon UV light irradiation. Typical results are shown in Fig. 9B. Fluorescence intensity at locations 1 and 2 in Fig. 9A underwent a substantial spike-like increase immediately after the UV light irradiation, followed by a decrease to the level below the initial intensity. This behavior is qualitatively independent from the location on the crystals, though it varies from one location to another. The fluorescence decay profile for the selected time region of the spike-like enhancement exhibited an increase in the lifetime of approximately 50% when compared with the lifetime before the UV light irradiation (Fig. 9C and Table 3). This increase in the fluorescence lifetime again supports the generation of fluorescent products, *i.e.*, fluorescein, upon UV light irradiation. The shorter lifetime compared with that of free fluorescein molecules in the bulk solution (4.0 ns) may stem from the electron transfer from excited chromophore to TiO_2 and/or Co species.[53] The subsequent decrease to the level below the initial intensity could be explained by the balance between the depletion of HPF molecules adsorbed on the surface by photooxidation, the dissociation of fluorescent products into the bulk solution, and the adsorption of HPF from the bulk solution.

Meanwhile, the time trace of the fluorescence intensity in solution at 1 μm distance from the edge of the crystal showed only the spike-like signal upon UV light irradiation (trace 3 in Fig. 9B). Quantitative analysis of the fluorescence decay profiles revealed significantly prolonged fluorescence lifetime upon the UV light irradiation (Fig. 9D and Table 3). Control experiments showed no detectable change in the fluorescence intensities and lifetimes of HPF in buffer solutions with and without UV light irradiation (Table 3). Thus, the notably different fluorescence lifetimes on the surface and in solution suggest that fluorescent products are present in different environments (Fig. 9C and D, and Table 3). To confirm the diffusion of fluorescent products from the crystal, we measured the fluorescence signals at different distances above the crystal. The fluorescence rise times upon UV light irradiation, which were analyzed by exponential fitting, clearly increase with increasing distance from the surface (Fig. S5†). The details of the diffusion processes are discussed in the ESI.

Conclusions

In summary, we studied the reaction dynamics of photogenerated charge carriers in CoPi-deposited TiO_2 using ensemble-averaged and single-particle spectroscopies. *In situ* single-particle fluorescence imaging technique with specific probes was served as an electrodeless analytical tool for monitoring the photooxidation reaction on individual catalysts. The combination of CoPi/Pt deposition and the anisotropic electron flow in the superstructure of $MesoTiO_2$ significantly retarded the charge recombination of h^+ and e^-, resulting in remarkably enhanced photooxidation activity. This is highly beneficial for developing novel photoactive materials for numerous applications, including photocatalysis for water splitting and environmental remediation. In principle, our strategy based on mesocrystal superstructures can be applied to a variety of semiconductor materials and their composites with co-catalysts. Further efforts are required to assemble the structures in photoelectrochemical cells for water splitting.

Acknowledgements

TEM observations were carried out in a facility at Research Center for Ultrahigh Voltage Electron Microscopy, Osaka University. T.M. thanks the World Class University program funded by the Ministry of Education, Science and Technology through the National Research Foundation of Korea (R31-2011-000-10035-0) for the support. This work has been partly supported by Innovative Project for Advanced Instruments, Renovation Center of Instruments for Science Education and Technology, Osaka University, and a Grant-in-Aid for Scientific Research (Projects 25220806, 25810114, and others) from the Ministry of Education, Culture, Sports, Science and Technology (MEXT) of the Japanese Government.

Notes and references

[a] *The Institute of Scientific and Industrial Research (SANKEN), Osaka University, Mihogaoka 8-1, Ibaraki, Osaka 567-0047, Japan. Fax: +81-6-6879-8499; Tel: +81-6-6879-8495; E-mail: tachi45@sanken.osaka-u.ac.jp (T.T.); majima@sanken.osaka-u.ac.jp (T.M.)*

[b] *PRESTO, Japan Science and Technology Agency (JST), 4-1-8 Honcho Kawaguchi, Saitama 332-0012, Japan. Fax: +81-6-6879-8499; Tel: +81-6-6879-8496; E-mail: tachi45@sanken.osaka-u.ac.jp (T.T.)*

† Electronic Supplementary Information (ESI) available: Experimental information and additional results. See DOI: 10.1039/b000000x/

1 M. R. Hoffmann, S. T. Martin, W. Choi and D. W. Bahnemann, *Chem. Rev.*, 1995, **95**, 69-96.
2 A. Hagfeldt and M. Grätzel, *Chem. Rev.*, 1995, **95**, 49-68.
3 M. G. Walter, E. L. Warren, J. R. McKone, S. W. Boettcher, Q. Mi, E. A. Santori and N. S. Lewis, *Chem. Rev.*, 2010, **110**, 6446-6473.
4 A. Kubacka, M. Fernández-García and G. Colón, *Chem. Rev.*, 2012, **112**, 1555-1614.
5 A. Kudo and Y. Miseki, *Chem. Soc. Rev.*, 2009, **38**, 253-278.
6 X. Chen, S. Shen, L. Guo and S. S. Mao, *Chem. Rev.*, 2010, **110**, 6503-6570.
7 T. Nakagawa, N. S. Bjorge and R. W. Murray, *J. Am. Chem. Soc.*, 2009, **131**, 15578-15579.
8 S. D. Tilley, M. Cornuz, K. Sivula and M. Grätzel, *Angew. Chem., Int. Ed.*, 2010, **49**, 6405-6408.
9 R. Abe, M. Higashi and K. Domen, *J. Am. Chem. Soc.*, 2010, **132**, 11828-11829.
10 A. Kay, I. Cesar and M. Grätzel, *J. Am. Chem. Soc.*, 2006, **128**, 15714-15721.
11 E. M. P. Steinmiller and K.-S. Choi, *Proc. Natl. Acad. Sci. U. S. A.*, 2009, **106**, 20633-20636.
12 D. K. Zhong, J. Sun, H. Inumaru and D. R. Gamelin, *J. Am. Chem. Soc.*, 2009, **131**, 6086-6087.
13 A. Fujishima, T. N. Rao and D. A. Tryk, *J. Photochem. Photobiol., C*, 2000, **1**, 1-21.
14 T. L. Thompson and J. T. Yates, Jr., *Chem. Rev.*, 2006, **106**, 4428-4453.
15 X. Chen and S. S. Mao, *Chem. Rev.*, 2007, **107**, 2891-2959.
16 U. Diebold, *Surf. Sci. Rep.*, 2003, **48**, 53-229.
17 H. Cölfen and M. Antonietti, *Angew. Chem., Int. Ed.*, 2005, **44**, 5576-5591.
18 L. Zhou and P. O'Brien, *J. Phys. Chem. Lett.*, 2012, **3**, 620-628.
19 Z. Bian, T. Tachikawa and T. Majima, *J. Phys. Chem. Lett.*, 2012, **3**, 1422-1427.
20 Z. Bian, T. Tachikawa, W. Kim, W. Choi and T. Majima, *J. Phys. Chem. C*, 2012, **116**, 25444-25453.

Journal of Materials Chemistry A Accepted Manuscript

21 M. W. Kanan and D. G. Nocera, *Science*, 2008, **321**, 1072-1075.

22 M. W. Kanan, Y. Surendranath and D. G. Nocera, *Chem. Soc. Rev.*, 2009, **38**, 109-114.

23 R. S. Khnayzer, M. W. Mara, J. Huang, M. L. Shelby, L. X. Chen and F. N. Castellano, *ACS Catal*, 2012, **2**, 2150-2160.

24 D. Liu, L. Jing, P. Luan, J. Tang and H. Fu, *ACS Appl. Mater. Interfaces*, 2013, **5**, 4046–4052.

25 B. Klahr, S. Gimenez, F. Fabregat-Santiago, J. Bisquert and T. W. Hamann, *J. Am. Chem. Soc.*, 2012, **134**, 16693-16700.

26 D. K. Zhong and D. R. Gamelin, *J. Am. Chem. Soc.*, 2010, **132**, 4202-4207.

27 D. K. Zhong, M. Cornuz, K. Sivula, M. Grätzel and D. R. Gamelin, *Energy Environ. Sci.*, 2011, **4**, 1759-1764.

28 K. J. McDonald and K.-S. Choi, *Chem. Mater.*, 2011, **23**, 1686-1693.

29 J. A. Seabold and K.-S. Choi, C *Chem. Mater.*, 2011, **23**, 1105-1112.

30 S. K. Pilli, T. E. Furtak, L. D. Brown, T. G. Deutsch, J. A. Turnerc and A. M. Herring, *Energy Environ. Sci.*, 2011, **4**, 5028-5034.

31 D. Wang, R. Li, J. Zhu, J. Shi, J. Han, X. Zong and C. Li, *J. Phys. Chem. C*, 2012, **116**, 5082-5089.

32 N. D. Morris and T. E. Mallouk, *J. Am. Chem. Soc.*, 2002, **124**, 11114-11121.

33 J. B. Gerken, J. Y. C. Chen, R. C. Masse, A. B. Powell and S. S. Stahl, *Angew. Chem., Int. Ed.*, 2012, **51**, 6676-6680.

34 C. N. P. d. Fonseca, M.-A. D. Paoli and A. Gorenstein, *Sol. Energy Mater. Sol. Cells*, 1994, **33**, 73-81.

35 T. Yoshihara, R. Katoh, A. Furube, Y. Tamaki, M. Murai, K. Hara, S. Murata, H. Arakawa and M. Tachiya, *J. Phys. Chem. B*, 2004, **108**, 3817-3823.

36 T. Tachikawa, M. Fujitsuka and T. Majima, *J. Phys. Chem. C*, 2007, **111**, 5259-5275.

37 A. J. Cowan, C. J. Barnett, S. R. Pendlebury, M. Barroso, K. Sivula, M. Grätzel, J. R. Durrant and D. R. Klug, *J. Am. Chem. Soc.*, 2011, **133**, 10134-10140.

38 G. Boschloo and D. Fitzmaurice, *J. Phys. Chem. B*, 1999, **103**, 7860-7868.

39 T. Tachikawa, S. Tojo, M. Fujitsuka, T. Sekino and T. Majima, *J. Phys. Chem. B*, 2006, **110**, 14055-14059.

40 R. F. Howe and M. Grätzel, *J. Phys. Chem.*, 1987, **91**, 3906-3909.

41 O. I. Micic, Y. Zhang, K. R. Cromack, A. D. Trifunac and M. C. Thurnauer, *J. Phys. Chem.*, 1993, **97**, 7277-7283.

42 R. F. Howe and M. Grätzel, *J. Phys. Chem.*, 1985, **89**, 4495-4499.

43 C. P. Kumar, N. O. Gopal, T. C. Wang, M.-S. Wong and S. C. Ke, *J. Phys. Chem. B*, 2006, **110**, 5223-5229.

44 J. G. McAlpin, Y. Surendranath, M. Dinca, T. A. Stich, S. A. Stoian, W. H. Casey, D. G. Nocera and R. D. Britt, *J. Am. Chem. Soc.*, 2010, **132**, 6882-6883.

45 D. Duonghong, J. Ramsden and M. Grätzel, *J. Am. Chem. Soc.*, 1982, **104**, 2977-2985.

46 T. Tachikawa, S. Yamashita and T. Majima, *Angew. Chem., Int. Ed.*, 2010, **49**, 432-435.

47 A. Harriman, *J. Phys. Chem.*, 1987, **91**, 6102-6104.

48 K. Naito, T. Tachikawa, M. Fujitsuka and T. Majima, *J. Am. Chem. Soc.*, 2009, **131**, 934-936.

49 B. M. Weckhuysen, *Angew. Chem., Int. Ed.*, 2009, **48**, 4910-4943.

50 T. Tachikawa and T. Majima, *Chem. Soc. Rev.*, 2010, **39**, 4802-4819.

51 H.-P. Wu, T.-L. Cheng and W.-L. Tseng, *Langmuir*, 2007, **23**, 7880-7885.

52 D. S. Banks and C. Fradin, *Biophys. J.*, 2005, **89**, 2960-2971.

53 G. Ramakrishna and H. N. Ghosh, *J. Phys. Chem. B*, 2001, **105**, 7000-7008.

Journal of Materials Chemistry A Accepted Manuscript

This journal is © The Royal Society of Chemistry [year]

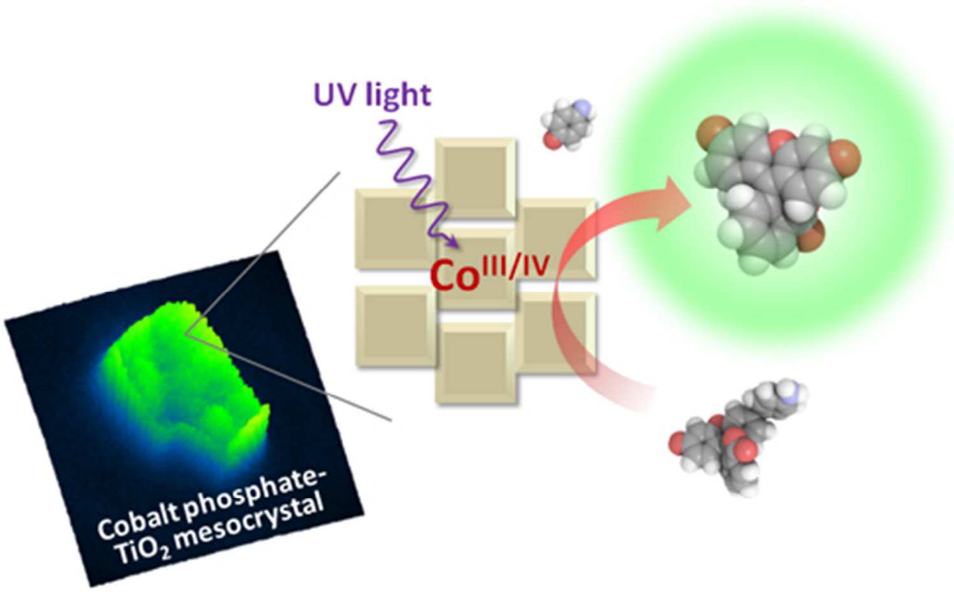

64x40mm (200 x 200 DPI)

Journal of Materials Chemistry A Accepted Manuscript